Composites Communications 25 (2021) 100679

Contents lists available at ScienceDirect

Composites Communications

journal homepage: www.elsevier.com/locate/coco

Porous polymer composite separators with three-dimensional ion-selective nanochannels for high-performance Li–S batteries

Yuyang Chen [a], Gangyong Zhou [a], Wei Zong [a], Yue Ouyang [a], Kai Chen [a], Yan Lv [a,**], Yue-E Miao [a,*], Tianxi Liu [a,b,***]

[a] State Key Laboratory for Modification of Chemical Fibers and Polymer Materials, College of Materials Science and Engineering, Innovation Center for Textile Science and Technology, Donghua University, Shanghai, 201620, PR China

[b] Key Laboratory of Synthetic and Biological Colloids, Ministry of Education, School of Chemical and Material Engineering, Jiangnan University, Wuxi, 214122, PR China

ARTICLE INFO

Keywords:
Porous separator
Polymer composite
Pore size regulation
Li–S batteries

ABSTRACT

Lithium-sulfur (Li–S) batteries have been regarded as one kind of the most attractive candidates for next-generation energy storage devices for their high theoretical energy density and fairly low cost. However, the "shuttle effect" caused by diffusion of soluble polysulfides and uncontrollable growth of lithium dendrite seriously deteriorate the long-term cycle stability and safety of Li–S batteries in practical applications. Herein, a highly porous polyvinyl alcohol (PVA)/sodium carboxylmethyl cellulose (CMC) composite separator with three-dimensional ion-selective nanochannels has been successfully fabricated via a facile non-solvent induced separation method. The abundant negative $-COO^-$ groups inside the nanochannels can hinder the undesired polysulfides penetrating through the separator, but allow Li^+ transporting rapidly and induce uniform lithium stripping/plating. As a result, the Li–S battery using the porous PVA/CMC composite separator realizes stable cycling with a low decay rate of 0.045% per cycle over 500 cycles at 1 C. This work offers a feasible strategy to design advanced multifunctional Li–S battery separators.

1. Introduction

On account of the low cost, high theoretical specific capacity (1675 mAh g^{-1}) and outstanding energy density (2600 Wh g^{-1}), lithium-sulfur (Li–S) batteries have been considered as one kind of the most potential next-generation energy storage devices to replace the conventional Li-ion batteries in the applications of portable electronics and new energy vehicles [1–4]. Nevertheless, Li–S batteries are still subject to some severe issues including (1) "shuttle effect" caused by the dissolution and diffusion of polysulfides in the ether-based electrolyte, which directly leads to rapid capacity fading and inferior cycling life, (2) low conductivity and high interface impedance due to the insulation nature of sulfur and Li_2S_2/Li_2S, and (3) dramatic structural destruction of metallic lithium anode resulted from the uncontrollable growth of lithium dendrite [5–7].

For the past few years, numerous research efforts have been put into solving the aforementioned problems. At the cathode side, researchers generally focus on boosting the interactions between polysulfides and the functional groups of cathode materials, such as nanosized inorganic materials [8,9], functional organic macromolecules [10–12] or porous carbon-sulfur composites [13–15]. At the anode side, establishing a robust solid electrolyte interface [16,17] (SEI) or preparing lithium alloy [18] as anode materials are commonly adopted as effective strategies to protect lithium anode from corrosion of polysulfides and lithium dendrite growth. Although the researches of cathode and anode modifications have been widely used for Li–S batteries, the complicated procedures and high cost usually limit their commercialized applications [19]. The separator, which is a vital part in liquid electrolyte systems, has profound effects on the electrochemical performance and safety of Li–S batteries. Polyolefin films are commonly used for Li-ion batteries owing to their good mechanical strength and appropriate chemical stability. However, it has been noted that polysulfides can

* Corresponding author.
** Corresponding author.
*** Corresponding author. State Key Laboratory for Modification of Chemical Fibers and Polymer Materials, College of Materials Science and Engineering, Innovation Center for Textile Science and Technology, Donghua University, Shanghai, 201620, PR China.
E-mail addresses: yanlv@dhu.edu.cn (Y. Lv), yuee_miao@dhu.edu.cn (Y.-E. Miao), txliu@dhu.edu.cn (T. Liu).

https://doi.org/10.1016/j.coco.2021.100679
Received 25 January 2021; Received in revised form 13 February 2021; Accepted 13 February 2021
Available online 2 March 2021

easily pass through the commercial polyolefin separators and react with the lithium anode, giving rise to undesirable parasitic reactions. Meanwhile, the problem of lithium dendrite growth is still unsolved. Furthermore, the low ionic conductivity, poor thermal stability and interfacial compatibility are significant problems decreasing the battery performance as well [20]. Therefore, it is an important target to develop new types of separators with characteristics of high-efficiency, facility and scalability for trapping polysulfides and transfer Li ions as well.

The development of cation-selective separators with enormous number of negative groups like $–SO_3^{2-}$ and $–COO^-$ has been recognized as effective approaches to block polysulfides from migrating toward the lithium anode by electrostatic repulsion interactions [21,22]. Besides, the cation-selective separator can provide obstruction for the movement of lithium salt anions, so as to promote the transference number of Li^+ [23]. For utilizing the advantages of negatively charged materials, a simple way is to construct a coating layer on the surface of polyolefin separators which works as the polysulfide shield. For example, Babu and co-workers prepared a permselective sulfonated poly(ether ether ketone) / Nafion coating separator to selectively allow Li^+ passing nonetheless the polysulfides are rejected [24]. Song et al. used a photografting method to obtain a carboxyl modified commercial polypropylene (PP) separator, which achieves a very low capacity loss of only 0.074% at 0.5 C for every cycle [25]. However, these strategies not only suffer from inferior interfacial adhesions between the polyolefin substrate and coating layer, but also reduce the energy density.

Sodium carboxylmethyl cellulose (CMC) is one of the most widely used polyelectrolyte cellulose derivatives for its low price. As an anionic polyelectrolyte, the plentiful negative charges of CMC are expected to retard the movement of polysulfides. However, cellulose and its derivatives are difficult to form porous membranes due to their poor mechanical properties such as severe brittleness, resulting in the degraded electrochemical performances [26]. Polyvinyl alcohol (PVA) is a considerable polymer to strengthen the porous membrane as skeleton owing to its wonderful film-forming performance, high mechanical strength and chemical stability [27,28]. Besides, the abundant hydroxyls can offer intense hydrogen bonding interactions between PVA and CMC, thus resulting in a physically cross-linked structure within the polymer chains to ensure the compatibility and additional strength of the separators.

Herein, PVA and CMC, which are both water-soluble, thermally stable, eco-friendly and low-cost, have been solution blended to prepare a highly porous PVA/CMC composite separator with three-dimensional (3D) nanochannels by the non-solvent induced phase separation (NIPS) method as illustrated in Fig. 1. The carboxylate groups of $–COO^-$ are uniformly distributed within the porous nanochannels to effectively prevent the migration of polysulfides. Secondly, the oxygen-containing $–COO^-$ groups and –OH groups can simultaneously regulate the deposition of Li^+ and promote Li^+ transport, thus effectively inhibiting the growth of lithium dendrites. As a result, the Li–S battery assembled with PVA/CMC composite separator at an optimized CMC content demonstrates ultra-stable cycling performance with a good capacity retention of 520.9 mAh g^{-1} after 500 cycles at 1 C and an ideal rate capacity of 523.6 mAh g^{-1} at 5 C.

2. Results and discussion

2.1. Physical and chemical properties of PVA/CMC separators

As demonstrated in Fig. 1, the non-solvent induced phase separation method, with the advantages of easy scalability, morphological controllability, and diverse selections of materials [29], is chosen for constructing the 3D nanochannels in PVA/CMC composite separators. Besides, to achieve appropriate porous structure and pore size, different compositions of PVA/CMC blends have been applied. As shown in Fig. S1, colorless and transparent solutions without visible phase separation are prepared to obtain the composite separators with different PVA/CMC ratios, which are signed as PC5, PC10, PC15 and PC20, respectively. According to previous reports [30], the entirely miscible blending systems will induce the information of sponge-like pores rather than finger-like voids via delayed mixing process, which can result in better mechanical strength for practical applications. Moreover, with the increasing components that are more immiscible with the non-solvent, the solvent-nonsolvent exchange rate will be further decreased, resulting in the generation of smaller nanochannels. The overall change trend of the porous structure and specific pore size distribution of PVA/CMC composite separators are depicted by scanning electron microscopy (SEM) and capillary flow porometry (CFP) tests, respectively. As presented in Figs. 2 and S2, when the mass ratio of CMC is lower than 5 wt%, the porous structure is irregular and cracks are visible on the top surface of PC5 (Fig. 2a) with partial non-porous areas. With the increasing content of CMC, the pores become smaller and uniform, accompanying with the compact sponge-like structure in the cross-sectional views (Fig. 2f–h), indicating that 3D nanochannels are built up by increasing the CMC content. CFP results confirm that the PVA/CMC composite separators with more CMC content possess smaller pore size (Fig. 2i–l). Hansen solubility parameter (HSP) is generally used to calculate the affinity between different materials. HSP includes the following three parts: a dispersion force component (δ_d), a polar

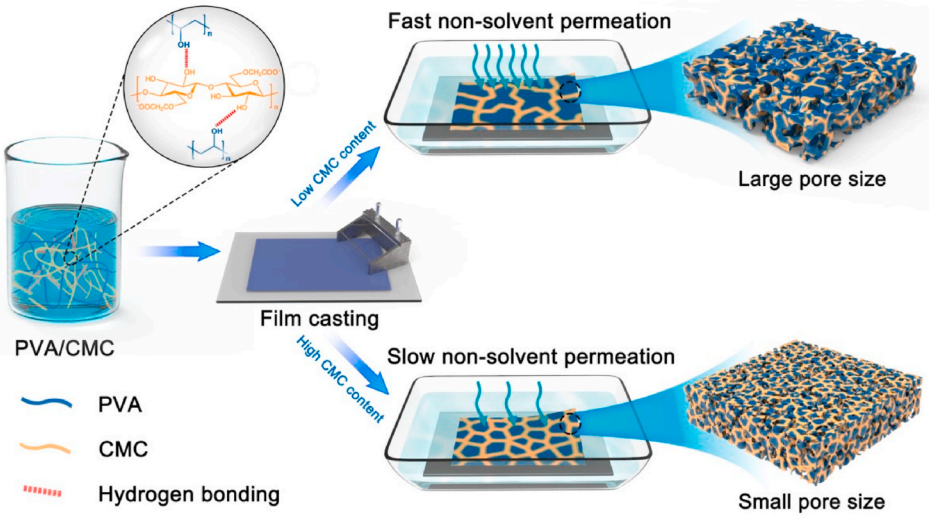

Fig. 1. The schematic illustration of the PVA/CMC composite separators.

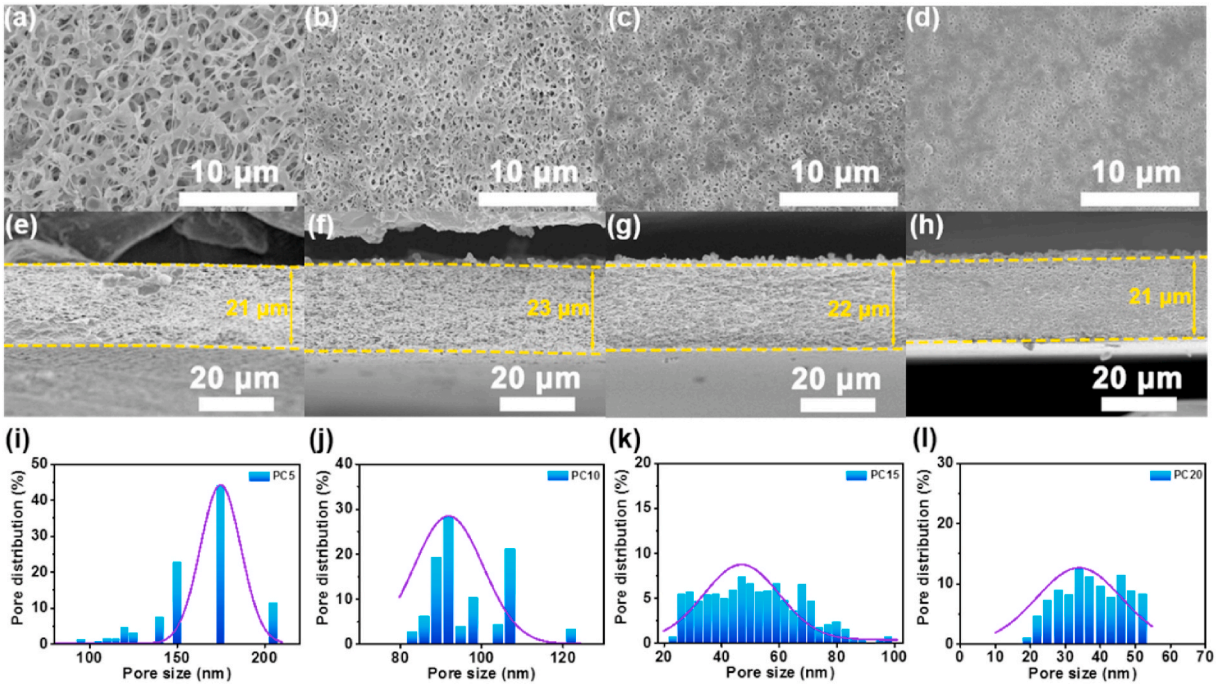

Fig. 2. The top-view and cross-view SEM images of (a, e) PC5, (b, f) PC10, (c, g) PC15 and (d, h) PC20 separators, respectively. (i–l) The corresponding pore size distributions of different separators.

component (δ_p), and a hydrogen bonding component (δ_h). In order to determine the solubility of a polymer in an organic solvent, HSP is calculated according to equation (1). Table S1 shows that the value of CMC-ethanol pair is larger than that of PVA-ethanol pair, which indicates that CMC is more immiscible with ethanol. Moreover, the incorporation of CMC results in higher viscosity of the polymer solution and stronger mico-crosslinking networks. Thus, the diffusion rate of ethanol into water is further decreased by the above factors, leading to the significant pore size reduction of PVA/CMC composite separators.

Porosity is an important parameter to evaluate the performance of separators. Herein, the porosity is tested by weighing the PVA/CMC composite separators before and after immersing in n-butanol as equation (2). It can be observed from Table S2, with the CMC concentration increasing from 5 wt% to 10 wt%, the porosity of PVA/CMC separators firstly increases from 54.5% to 63.3% due to the information of 3D nanochannels. Then, resulted from the gradual densification of the porous structure, it decreases to 48.8% when the CMC content is further increased to 20 wt%, but still being higher than that (40.3%) of the PP separator. Due to the low surface energy and hydrophobic characteristics, the compatibility between PP separator and conventional liquid electrolyte is essentially poor. As verified by the contact angle measurements in Fig. S3, the PP separator exhibits poor wettability to electrolyte with an inferior contact angle of 50.5°. In contrast, all the PC5, PC10, PC15 and PC20 separators can be readily wetted by electrolyte with the contact angles of 10.5°, 8.6°, 9.0° and 16.9°, respectively. To further investigate the electrolyte affinity of PVA/CMC composite separators, the electrolyte uptake and retention properties are obtained. As shown in Fig. S4a, the electrolyte uptake value of PC15 is the highest after 50 min, while the electrolyte retention value of PC20 is much superior. It's worth noting that the electrolyte absorbed by PP separator completely evaporates but still remains in all of PVA/CMC separators after 400 min (Fig. S4b), confirming that PVA/CMC composite separators can accelerate the permeation of electrolyte and ensure the good contact between electrolyte and electrode.

The thermal stability of separators is another concern regarding battery safety performance. Fig. S5a shows the thermogravimetric analysis (TGA) curves of PVA, CMC and PVA/CMC composite separators. The pristine PVA exhibits inferior thermal stability with a low decomposition temperature at 230 °C, whereas the separators incorporated with CMC show much higher decomposition temperature compared to that of pure PVA. The optical images of PVA/CMC and PP separators before and after heating at 170 °C are shown in Fig. S5b. Obviously, the negligible thermal shrinkage with almost no shape change confirms the excellent thermal stability of PVA/CMC separators, as compared to the PP separator which is melt and suffers severe dimensional shrinkage under the same condition. The thermal behavior of the composite separators, are further depicted by differential scanning calorimeter (DSC) analysis (Fig. S6). There are one narrow and one broad endothermic peak for pristine PVA respectively, corresponding to the melting phase transition and glass transition at 87 °C. On the other hand, CMC exhibits a broad endothermic peak referring to the overlapping T_g and T_m of its semi-crystalline nature [31]. The glass transition position of PVA/CMC composite separators is turned into a broad endothermic peak and moves toward the low temperature region, which demonstrates the decreased crystallinity, good compatibility and hydrogen bonding interactions between PVA and CMC [32–34].

X-ray diffractometer (XRD) patterns further manifests the transformation of crystallinity with different CMC contents (Fig. S7a). A board diffraction peak appears at $2\theta = 20.2°$ for CMC while PVA has a sharp diffraction peak at $2\theta = 19.8°$ with two board diffraction peaks at $2\theta = 22.4°$ and 40.8°. On the other hand, the PVA/CMC composite separators show similar crystal structure with two board diffraction peaks at $2\theta = 19.0°$ and 22.3°. The increased amorphous region of PVA/CMC composite separators indicates that the addition of CMC greatly reduces the crystallinity of PVA/CMC composites, which may provide a better ionic conductivity for lithium batteries [35]. Fourier transform infrared (FTIR) spectra demonstrates the intermolecular hydrogen bonding interactions between PVA and CMC (Fig. S7b). The pure CMC shows a broad strong band appearing at 3428 cm^{-1} which is assigned to the –OH stretching vibration, while the asymmetric stretching vibration of –C═O is observed at 1646 cm^{-1}. For PVA/CMC composites, both of the –OH and –C═O characteristic peaks are shift into lower wavenumbers, indicating that the composites are affected by the intermolecular hydrogen bonding interaction which reduces the force constants

of –OH and –C═O groups [33,36].

A mechanically robust separator can undergo high tension after casual collisions and reduce the possibility of internal short-circuits caused by the rough electrode surface and growth of lithium dendrite. To evaluate the mechanical strength of PVA/CMC composite separators, stress-strain curves are depicted in Fig. S8a. It is clearly demonstrated that the introduction of a certain amount of CMC has positive effects on the strength of the composite separators. The commercial PP separator presents an obvious orientation with a minimal tensile strength of 13.5 MPa and Young's modulus of 340 MPa at one direction, and a maximum tensile strength of 84.9 MPa and Young's modulus of 808.0 MPa at the other direction. The tensile strength of PVA, PC5, PC10 and PC15 separators are 4.20, 11.4, 15.4 and 21.2 MPa, respectively, with the corresponding Young's modulus of 259, 284, 384 and 889 MPa. However, the tensile strength and Young's modulus of PC20 decrease to 16.7 MPa and 883 MPa, which is resulted from the poor mechanical property of CMC. Nonetheless, the tensile strength of PC20 separator is not inferior to PP and PVA separators. Benefitting from the amorphous phase structure, the elongation at break of PVA/CMC composite separators are all much higher than that of PP separator except for PC20 separator, which is crucial to resist the penetration of lithium dendrite [37].

In order to verify the efficiency of polysulfide obstruction by the PVA/CMC composite separators, polysulfide permeation tests are conducted as shown in Fig. 3a. The PC15 separator is selected as the experimental group because of its suitable porous structure and sufficient mechanical strength. To be noticed, at a relatively high polysulfide concentration, the polysulfides easily diffuse across the separator into the originally colorless blank electrolyte in the opposite chamber with PP separator even at 0 h. Conversely, the PC15 separator shows a much slower polysulfide permeation rate with almost invisible color change of the blank electrolyte after 24 h. The UV–vis test of the electrolyte obtained at each point-in-time further verifies the very low absorbance intensity of diverse polysulfides in electrolyte after 8 h by using PC15 separator (Fig. 3b), demonstrating efficiently inhibited polysulfide diffusion by the coulombic interactions between $–COO^-$ groups and polysulfide anions within the 3D nanochannels as illustrated in Fig. 3c.

2.2. Electrochemical properties of PVA/CMC composite separators

Cyclic voltammetry (CV) profiles for the batteries assembled with PP and PC15 separators are presented in Fig. 4. Two reduction peaks can be clearly observed at about 2.3 V and 2.0 V, which represent the transformation of elemental sulfur to long-chain polysulfides (Li_2S_n, $4 < n < 8$) and soluble polysulfides to solid lithium sulfides (Li_2S_2/Li_2S),

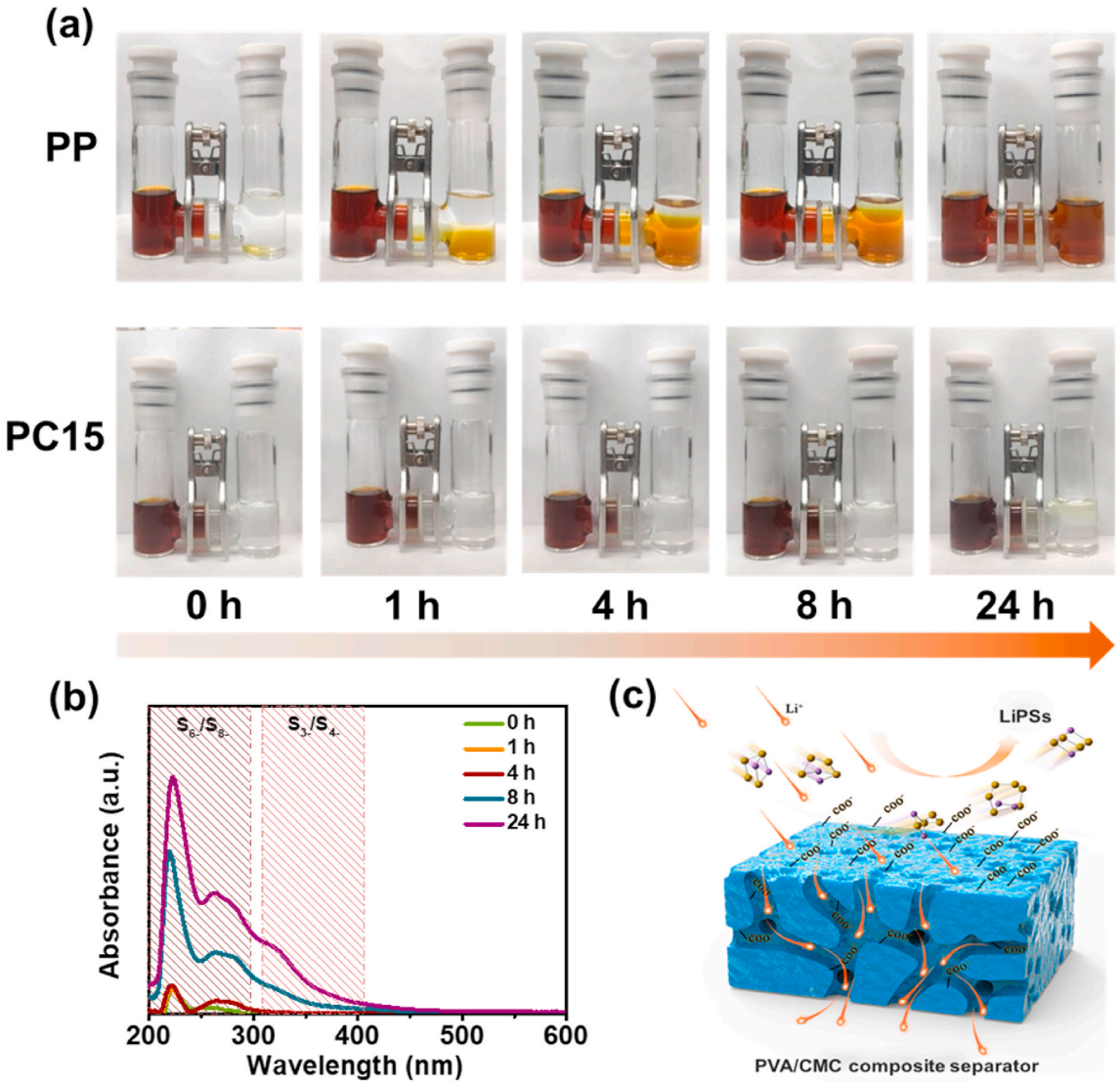

Fig. 3. (a) Polysulfide permeation measurements of PP and PC15 separators at varied time. (b) UV–vis spectra of pure electrolyte solution within electrolytic tank of PC15 separator in each point-in-time. (c) Illustration of polysulfide rejection by the 3D ion-selective nanochannels of PVA/CMC composite separators.

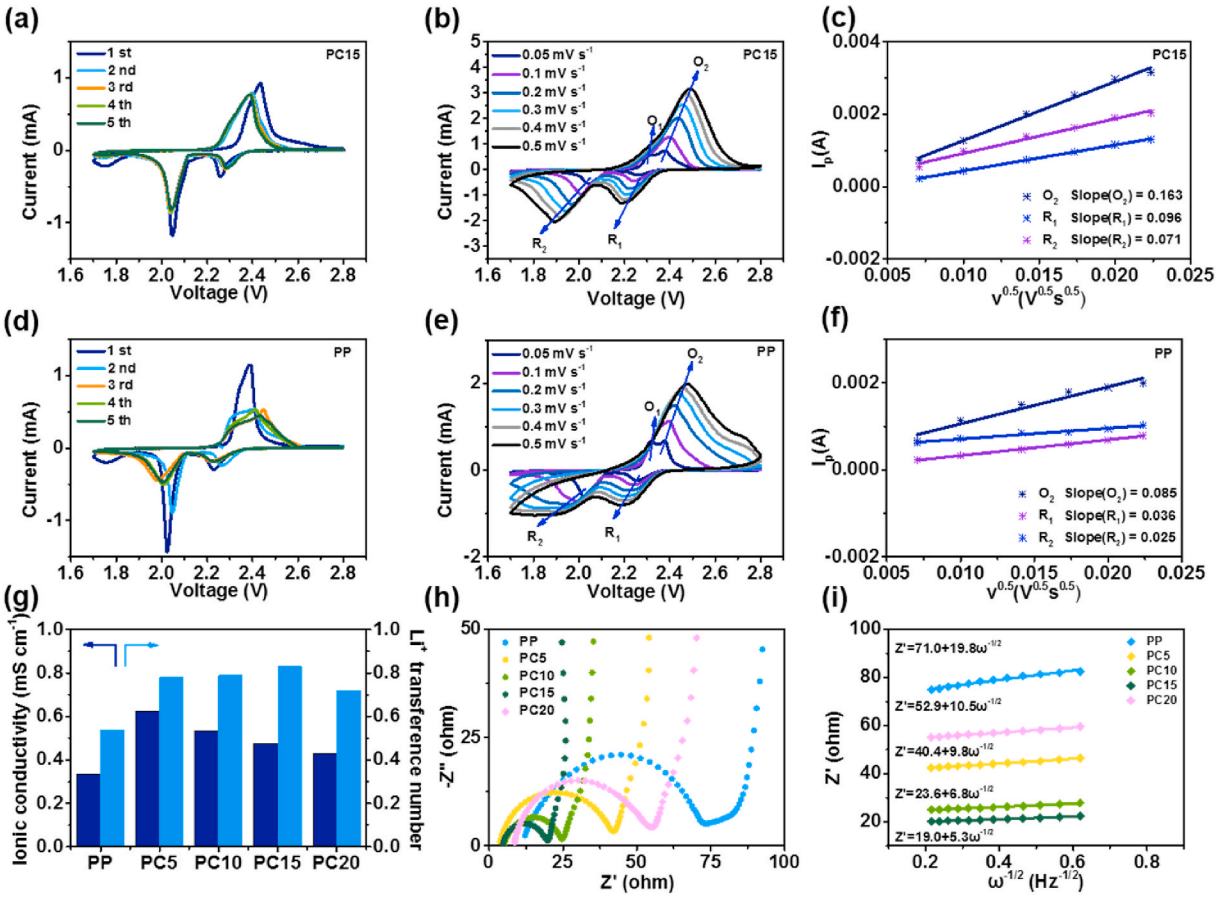

Fig. 4. (a, d) CV curves of the first five cycles, (b, e) CV curves at various voltage scan rates, and (c, f) the corresponding linear fits of the peak currents in each voltage scan rate of PP and PC15 separators. (g) Ionic conductivity and lithium transference number, (h) Nyquist plots, and (i) Relationship between Z' and $\omega^{-1/2}$ in the low-frequency region in EIS test of PP, PC5, PC10, PC15 and PC20 separators, respectively.

respectively [38]. In the part of anodic scan, an overlapping oxidation peak appears at about 2.5 V, which is associated with the conversion of different polysulfide species into elemental sulfur. Meanwhile, the weak peak around 1.75 V is attributed to the reaction of $LiNO_3$ in the initial cycle [39]. Impressively, the cell with PC15 separator exhibits lower voltage gap than those of PP separator, indicating that the PC15 separator can reduce polarization and provide better stability and reversibility for Li–S batteries [39]. Furthermore, with the increase of scan rate, the oxidation peaks of the cell with PC15 separator shift to higher potentials while the reduction peaks shift to lower potentials in Fig. 4b. However, the cell with PP separator suffers from severe polarization on account of the slow reaction kinetics (Fig. 4e). The Li^+ diffusion coefficients (D_{Li+}) of the separators are also calculated by fitting the peak current of the CV curves with different scan rates by Randles-Sevcik equation [40,41]. As shown in Fig. 4c and f, the slope of each fitting curve for cells with PC15 are all higher than those of the cells with PP separator, revealing a higher D_{Li+} value. Besides, the D_{Li+} values of other cells with PC5, PC10 and PC20 separators are all higher than that with PP separator (Fig. S9), demonstrating the 3D nanochannels can facilitate Li^+ transfer.

To further investigate the ionic conductivity, Nyquist plots of the separators are shown in Fig. S10, which present straight lines in the high frequency region. The ionic conductivity of PC5, PC10, PC15 and PC20 separators are obtained from Z'-intercept according to the extrapolation method which reach 0.62, 0.54, 0.48 and 0.43 mS cm^{-1} respectively, being much higher than that (0.33 mS cm^{-1}) of PP separator (Fig. 4g). Furthermore, the Li^+ transference number of PC5, PC10, PC15 and PC20 separators are 0.78, 0.79, 0.83 and 0.72 respectively (Figs. 4g and S11), being much higher than that (0.54) of PP separator. The above results strongly prove that the introduction of $–COO^-$ groups can improve the transfer ability of Li^+, thus effectively inhibiting the growth of lithium dendrite according to the Chazalviel's model [42,43].

In the Li–S batteries, the interfacial property plays the key role in the electrochemical performance. As shown in Fig. 4h, the bulk resistances (R_b) of the cells with PC5, PC10, PC15 and PC20 separators before cycling are only 3.0, 5.0, 4.6 and 8.0 Ω, respectively, which are all significantly lower than that (11.1 Ω) of PP separator. Additionally, the cells assembled with PC5, PC10, PC15 and PC20 separators present quite low interfacial resistance (R_{ct}) of 42.9, 19.1, 14.7 and 45.3 Ω, respectively. Compared to the R_{ct} (61.6 Ω) of PP separator, the dramatically reduced semicircle part suggests that the interfacial ion transfer of the cells are faster when PVA/CMC composite separators are used. Besides, the Li^+ diffusion coefficients of PVA/CMC composite separators calculated by equation (5) are well matched with the Li^+ diffusion coefficients calculated by CV curves (Fig. 4i and Table S4), which further verify that the polar functional $–COO^-$ can facilitate Li^+ transport [44].

Galvanostatic charge-discharge tests of the Li–S batteries are firstly carried out at 0.1 C. As shown in Fig. 5a-c, owing to the satisfactory interfacial contact and attenuated polarization, the cell with PC15 separator delivers a high initial capacity of 1392 mAh g^{-1}, which is consisted of a short and high plateau (Q_H = 344 mAh g^{-1}) as well as a long and low plateau (Q_L = 1048 mAh g^{-1}) corresponding to the two reduction peaks in CV curves, and being higher than those of PP separator (Q_H = 327 mAh g^{-1}, Q_L = 896 mAh g^{-1}). Besides, the relatively high capacity retention of the cell with PC15 separator in the first three cycles suggests the efficient suppression of polysulfide permeation during the cycles. The rate performance is an important criterion in the assessment of electrochemical performance of Li–S batteries. As

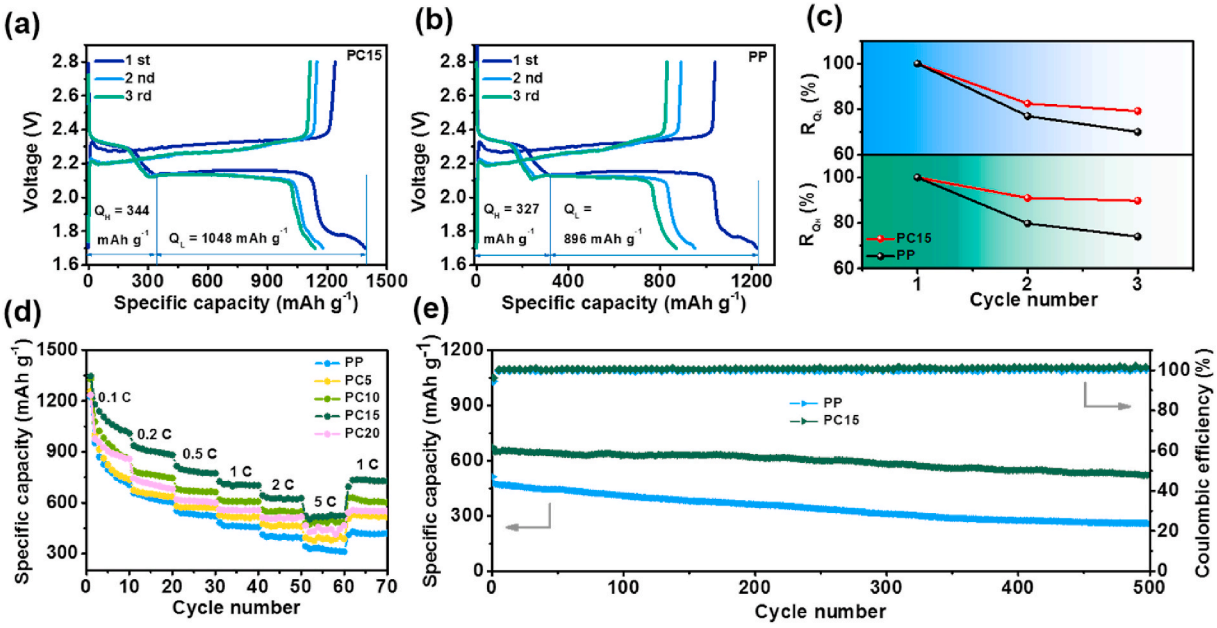

Fig. 5. The first three charge/discharge voltage curves for cells with (a) PC15 separator, (b) PP separator and (c) R_{QL} and R_{QH} of the cells with PP and PC15 separators, respectively. (d) Rate performance for cells with different separators at various current rates. (e) Galvanostatic cycling performance at 1 C for cells with PP and PC15 separators.

presented in Fig. 5d, at different scan rates of 0.1, 0.2, 0.5, 1, 2 and 5 C, the specific capacities of the cells with PVA/CMC separators are all much higher than that of PP separator. Especially, the cell with PC15 separator reaches the high specific capacities of 711.8, 624.4 and 523.6 mAh g^{-1} at 1, 2 and 5 C, respectively. Furthermore, after the high current density cycling at 5 C, the cell with PC15 separator recovers to 736.2 mAh g^{-1} at the following 1 C cycling, manifesting that PC15 separator can endow the Li–S battery with outstanding reversibility. Besides, resulting from the decreased interfacial resistance and faster Li^+ transport, the over potential of the cell with PC15 separator at 5 C is 480 mV (Fig. S12a), being dramatically lower than that (638 mV) of PP separator (Fig. S12b).

Fig. S12c reveals the cycling performance of the cells with diverse separators at a low current density of 0.2 C. After 200 cycles, the cells with PP, PC5, PC10, PC15 and PC20 separators maintain the capacity of 322.5, 485.2, 643.9, 466.2 and 252.2 mAh g^{-1}, respectively. Particularly, the enhanced rejection ability of PVA/CMC separators toward polysulfides appears only in the CMC content range of 5–15 wt%, which can be attributed to the decreased pore size and increased $–COO^-$ content of the separators. For the cells with PC20 separator, even though the pore size fairly decreases, the poor mechanical strength may cause the destruction of porous structure in the cycling process and result in the undesired capacity fading. In the long-term cycle at 1 C, a remarkably low specific capacity attenuation rate of 0.045% per cycle is observed for the cell with PC15 separator with a high specific capacity of 520.9 mAh g^{-1} and a high coulombic efficiency (>99.1%) after 500 cycles, which is evidently much better than other previously reported studies (Table S5). By contrast, the cell with PP separator only maintains a low capacity of 259.4 mAh g^{-1}, further demonstrating that the negative $–COO^-$ groups on the surface of the well-tailored 3D ion-selective nanochannels can efficiently suppress the shuttle effect of polysulfides.

After 100 cycles at 1 C, the morphology of lithium anode is examined by SEM. The lithium surface of the cell with PC15 keeps smooth and integrity, indicating that polysulfides are confined to the cathode side (Fig. S13a). In sharp contrast, the lithium surface of the cell with PP separator is acutely corroded by polysulfides (Fig. S13b) compared to the pristine lithium anode (Fig. S13c). EDS mapping results demonstrate that almost no sulfur signal is found on the lithium anode surface for the cell with PC15 separator, whereas Li_2S deposits on the lithium anode surface in the cell with PP separator, indicating that the 3D ion-selective nanochannels can serve as a strong polysulfide barrier. Fig. S14 further shows the morphology of PC15 separator after cycling. The porous structure remains intact while the anode side of the separator keeps its pristine color without any deposition of polysulfides, proving the excellent stability of the PVA/CMC separator during long-term cycling process. To further investigate the suppressing effect of lithium dendrite growth with PC15 separator, the long-term galvanostatic cycling test with symmetrical cells of Li//separator//Li is carried out at various current densities. As shown in Figs. S15a and S15b, benefitting from the high Li^+ transfer and lithiophilic groups [45,46], the symmetric cell with PC15 separator displays a relatively low overpotential and outstanding stability at the current density of 1 and 2 mA cm^{-2}. On the contrary, the overpotential of the cell with PP separator continuously increases, which can be explained by the severe electrolyte decomposition during the lithium dendrite growth process [47,48]. Fig. S15c shows that at different current densities of 0.5, 1, 2 and 5 mA cm^{-2} with a constant capacity of 1 mAh cm^{-2}, the cell with PC15 separator still maintains a low overpotential without voltage fluctuation, especially at high current densities. This is also consistent with the smooth, uniform and compact morphology of the lithium anode of the cell with PC15 separator as shown in Fig. S16a. However, the lithium anode is covered with mossy-like and nodule-like lithium dendrites with PP separator (Fig. S16b). Therefore, the PVA/CMC composite separators can play a crucial part in obstructing shuttle effect and suppressing lithium dendrite for high-perfromance Li–S battery applications.

3. Conclusions

In summary, 3D ion-selective nanochannels have been constructed in the PVA/CMC composite separators for simultaneous polysulfide rejection and lithium dendrite suppression via NIPS method towards scalable Li–S battery applications. The tailored pore size which is obtained through increasing CMC content, together with increased $–COO^-$ negative groups synergistically suppress the shuttle effect of polysulfides in cells with PC15 separator. On the other hand, the high Li^+ transference number and lithiophilic oxygen groups promote the uniform Li

stripping/plating even at high current densities and achieve the long-life cycle with a smaller overpotential. As a result, the Li–S battery assembled with PC15 separator displays a high initial discharge capacity of 1392 mAh g^{-1} at 0.1 C, an outstanding rate capability of 523.6 mAh g^{-1} at 5 C, and a reversible capacity of 520.9 mAh g^{-1} after 500 cycles at 1 C with a prominent capacity retention of 0.045% per cycle. This concept from the content tuning of CMC in PVA/CMC composite separators paves a simple and efficient pathway toward low-cost, scalable and ultra-stable advanced Li–S batteries.

CRediT authorship contribution statement

Yuyang Chen: Conceptualization, Methodology, Investigation, Formal analysis, Data curation, Visualization, Writing – original draft, Writing – review & editing. **Gangyong Zhou:** Investigation. **Wei Zong:** Investigation. **Yue Ouyang:** Investigation. **Kai Chen:** Investigation. **Yan Lv:** Writing – review & editing, Supervision, Funding acquisition. **Yue-E Miao:** Writing – review & editing, Supervision, Funding acquisition. **Tianxi Liu:** Writing – review & editing, Supervision, Funding acquisition.

Declaration of competing interest

The authors declare that they have no known competing financial interests or personal relationships that could have appeared to influence the work reported in this paper.

Acknowledgements

The authors are grateful for the financial support from the National Natural Science Foundation of China (22075042), Natural Science Foundation of Shanghai (20ZR1401400, 18ZR1401600), the Shanghai Scientific and Technological Innovation Project (18JC1410600).

Appendix A. Supplementary data

Supplementary data to this article can be found online at https://doi.org/10.1016/j.coco.2021.100679.

References

[1] J.M. Ma, Y.T. Li, N. Grundish, J.B. Goodenough, Y.H. Chen, L.M. Guo, Z.Q. Peng, X. Q. Qi, F.Y. Yang, L. Qie, C.G. Wang, B. Huang, Z.Y. Huang, L.H. Chen, D.W. Su, G. X. Wang, X.W. Peng, Z.H. Chen, J.L. Yang, S. M He, X. Zhang, H.J. Yu, C.P. Fu, M. Jiang, W.Z. Deng, C.F. Sun, Q.G. Pan, Y.B. Tang, X.F. Li, X.L. Ji, F. Wang, Z. Q. Niu, F. Lian, C.Y. Wang, G.G. Wallace, M. Fan, Q.H. Meng, S. Xin, Y.G. Guo, L. J. Wan, The 2020 battery technology roadmap, J. Phys. D Appl. Phys. (2020), https://doi.org/10.1088/1361-6463/abd353.

[2] Z.W. Seh, Y.M. Sun, Q.F. Zhang, Y. Cui, Designing high-energy lithium-sulfur batteries, Chem. Soc. Rev. 45 (2016) 5605–5634.

[3] L. Fan, M. Li, X. Li, W. Xiao, Z. Chen, J. Lu, Interlayer material selection for lithium-sulfur batteries, Joule 3 (2019) 361–386.

[4] B. Dunn, H. Kamath, J.M. Tarascon, Electrical energy storage for the grid: a battery of choices, Science 334 (2011) 928.

[5] W. Ren, W. Ma, S. Zhang, B. Tang, Recent advances in shuttle effect inhibition for lithium sulfur batteries, Energy Storage Mater 23 (2019) 707–732.

[6] L. Kong, B.Q. Li, H.J. Peng, R. Zhang, J. Xie, J.Q. Huang, Q. Zhang, Porphyrin-derived graphene-based nanosheets enabling strong polysulfide chemisorption and rapid kinetics in lithium-sulfur batteries, Adv. Energy Mater. 8 (2018) 1800849.

[7] J. He, A. Manthiram, Long-life, high-rate lithium-sulfur cells with a carbon-free vn host as an efficient polysulfide adsorbent and lithium dendrite inhibitor, Adv. Energy Mater. 10 (2019) 1903241.

[8] X.Q. Niu, X.L. Wang, D. Xie, D.H. Wang, Y.D. Zhang, Y. Li, T. Yu, J.P. Tu, Nickel hydroxide-modified sulfur/carbon composite as a high-performance cathode material for lithium sulfur battery, ACS Appl. Mater. Interfaces 7 (2015) 16715–16722.

[9] Q. Pang, D. Kundu, M. Cuisinier, L.F. Nazar, Surface-enhanced redox chemistry of polysulphides on a metallic and polar host for lithium-sulphur batteries, Nat. Commun. 5 (2014) 4759.

[10] W. Wei, P. Du, D. Liu, Q. Wang, P. Liu, Facile one-pot synthesis of well-defined coaxial sulfur/polypyrrole tubular nanocomposites as cathodes for long-cycling lithium-sulfur batteries, Nanoscale 10 (2018) 13037–13044.

[11] P. Zhu, J. Zhu, C. Yan, M. Dirican, J. Zang, H. Jia, Y. Li, Y. Kiyak, H. Tan, X. Zhang, In situ polymerization of nanostructured conductive polymer on 3d sulfur/carbon nanofiber composite network as cathode for high-performance lithium-sulfur batteries, Adv. Mater. Interfaces 5 (2018) 1701598.

[12] J. Yu, S. Liu, G.G. Duan, H. Fang, H.Q. Hou, Dense and thin coating of gel polymer electrolyte on sulfur cathode toward high performance Li-sulfur battery, Compos. Commun. 19 (2020) 239–245.

[13] G. Hu, C. Xu, Z. Sun, S. Wang, H.M. Cheng, F. Li, W. Ren, 3D Graphene-foam-reduced-graphene-oxide hybrid nested hierarchical networks for high-performance Li-S Batteries, Adv. Mater. 28 (2016) 1603–1609.

[14] M. Gao, C. Su, M. He, T. Glossmann, A. Hintennach, Z. Feng, Y. Huang, Z. Zhang, A high performance lithium-sulfur battery enabled by a fish-scale porous carbon/sulfur composite and symmetric fluorinated diethoxyethane electrolyte, J. Mater. Chem. 5 (2017) 6725–6733.

[15] J. Li, W. Wei, L. Meng, Liquid-phase exfoliated-graphene-supporting nanostructural sulfur as high-performance lithium-sulfur batteries cathode, Compos. Commun. 15 (2019) 149–154.

[16] S. Li, H. Dai, Y. Li, C. Lai, J. Wang, F. Huo, C. Wang, Designing Li-protective layer via $SOCl_2$ additive for stabilizing lithium-sulfur battery, Energy Storage Mater 18 (2019) 222–228.

[17] M.L. Sun, X. Wang, J. Wang, H. Yang, L.N. Wang, T.X. Liu, Assessment on the Self-discharge behavior of lithium-sulfur batteries with $LiNO_3$-possessing electrolytes, ACS Appl. Mater. Interfaces (2018) 35175–35183.

[18] L.L. Kong, L. Wang, Z.C. Ni, S. Liu, G.R. Li, X.P. Gao, Lithium-magnesium alloy as a stable anode for lithium-sulfur battery, Adv. Funct. Mater. 29 (2019) 1808756.

[19] F. Li, Q. Liu, J. Hu, Y. Feng, P. He, J. Ma, Recent advances in cathode materials for rechargeable lithium-sulfur batteries, Nanoscale 11 (2019) 15418–15439.

[20] J. Zhu, M. Yanilmaz, K. Fu, C. Chen, Y. Lu, Y. Ge, D. Kim, X. Zhang, Understanding glass fiber membrane used as a novel separator for lithium-sulfur batteries, J. Membr. Sci. 504 (2016) 89–96.

[21] T.Z. Zhuang, J.Q. Huang, H.J. Peng, L.Y. He, X.B. Cheng, C.M. Chen, Q. Zhang, Rational integration of polypropylene/graphene oxide/nafion as ternary-layered separator to retard the shuttle of polysulfides for lithium-sulfur batteries, Small 12 (2016) 381–389.

[22] J. Song, H. Noh, H. Lee, J.N. Lee, D.J. Lee, Y. Lee, C.H. Kim, Y.M. Lee, J.K. Park, H. T. Kim, Polysulfide rejection layer from alpha-lipoic acid for high performance lithium-sulfur battery, J. Mater. Chem. 3 (2015) 323–330.

[23] C.E. Lin, H. Zhang, Y.Z. Song, Y. Zhang, J.J. Yuan, B.K. Zhu, Carboxylated polyimide separator with excellent lithium ion transport properties for a high-power density lithium-ion battery, J. Mater. Chem. 6 (2018) 991–998.

[24] D.B. Babu, K. Giribabu, K. Ramesha, Permselective SPEEK/nafion composite-coated separator as a potential polysulfide crossover barrier layer for Li-S Batteries, ACS Appl. Mater. Interfaces 10 (2018) 19721–19729.

[25] S.L. Song, L. Shi, S.Y. Lu, Y.C. Pang, Y.K. Wang, M. Zhu, D.W. Ding, S.J. Ding, A new polysulfide blocker-poly(acrylic acid) modified separator for improved performance of lithium-sulfur battery, J. Membr. Sci. 563 (2018) 277–283.

[26] B. Wang, X. Yang, C. Qiao, Y. Li, T. Li, C. Xu, Effects of chitosan quaternary ammonium salt on the physicochemical properties of sodium carboxymethyl cellulose-based films, Carbohydr. Polym. 184 (2018) 37–46.

[27] W. Xiao, L.N. Zhao, Y.Q. Gong, J.G. Liu, C.W. Yan, Preparation and performance of poly(vinyl alcohol) porous separator for lithium-ion batteries, J. Membr. Sci. 487 (2015) 221–228.

[28] J. Huang, H. Yu, S.Y.H. Abdalkarim, J. Marek, J. Militky, Y. Li, J. Yao, Electrospun polyethylene glycol/polyvinyl alcohol composite nanofibrous membranes as shape-stabilized solid-solid phase change materials, Adv. Fiber Mater. 2 (2020) 167–177.

[29] S. Yoo, J.H. Kim, M. Shin, H. Park, J.H. Kim, S.Y. Lee, S. Park, Hierarchical multiscale hyperporous block copolymer membranes via tunable dual-phase separation, Sci. Adv. 1 (2015), e1500101.

[30] S. Li, Z. Cui, L. Zhang, B. He, J. Li, The effect of sulfonated polysulfone on the compatibility and structure of polyethersulfone-based blend membranes, J. Membr. Sci. 513 (2016) 1–11.

[31] S. El-Sayed, K.H. Mahmoud, A.A. Fatah, A. Hassen, DSC, TGA and dielectric properties of carboxymethyl cellulose/polyvinyl alcohol blends, Physica B 406 (2011) 4068–4076.

[32] O.W. Guirguis, M.T.H. Moselhey, Thermal and structural studies of poly (vinyl alcohol) and hydroxypropyl cellulose blends, Nat. Sci. (2012) 57–67, 04.

[33] M.A. Saadiah, D. Zhang, Y. Nagao, S.K. Muzakir, A.S. Samsudin, Reducing crystallinity on thin film based CMC/PVA hybrid polymer for application as a host in polymer electrolytes, J. Non-Cryst. Solids 511 (2019) 201–211.

[34] J. Li, J. Sun, D. Wu, W. Huang, M. Zhu, E. Reichmanis, S. Yang, Functionalization-directed stabilization of hydrogen-bonded polymer complex fibers: elasticity and conductivity, Adv. Fiber Mater. 1 (2019) 71–81.

[35] A.A. Mohamad, N.S. Mohamed, M.Z.A. Yahya, R. Othman, S. Ramesh, Y. Alias, A. K. Arof, Ionic conductivity studies of poly(vinyl alcohol) alkaline solid polymer electrolyte and its use in nickel-zinc cells, Solid State Ionics 156 (2003) 171–177.

[36] T. Liu, X. Peng, Y.-N. Chen, Q.-W. Bai, C. Shang, L. Zhang, H. Wang, Hydrogen-bonded polymer-small molecule complexes with tunable mechanical properties, Macromol. Rapid Commun. 39 (2018) 1800050.

[37] J. Kang, D. Chen, B. Xiong, N. Zheng, F. Yang, M. Xiang, Z. Zheng, Facile route for the fabrication of polypropylene separators for lithium-ion batteries with high elongation and strong puncture resistance, Ind. Eng. Chem. Res. 58 (2019) 23135–23142.

[38] Y. Yang, J. Zhang, Highly stable lithium-sulfur batteries based on laponite nanosheet-coated celgard separators, Adv. Energy Mater. 8 (2018) 1801778.

[39] S.S. Zhang, Role of $LiNO_3$ in rechargeable lithium/sulfur battery, Electrochim. Acta 70 (2012) 344–348.
[40] G.Y. Zhou, L.L. Mo, C.Y. Zhou, Y. Lv, Y.E. Miao, T.X. Liu, Flexible naphthalene-based polyimide nanofiber cathode with hierarchical micro/nanoporous structure for high-performance organic sodium-ion batteries, Compos. Commun. 22 (2020) 100490.
[41] H. Kim, J. Lee, H. Ahn, O. Kim, M.J. Park, Synthesis of three-dimensionally interconnected sulfur-rich polymers for cathode materials of high-rate lithium-sulfur batteries, Nat. Commun. 6 (2015) 7278.
[42] M.D. Tikekar, S. Choudhury, Z. Tu, L.A. Archer, Design principles for electrolytes and interfaces for stable lithium-metal batteries, Nat. Energy 1 (2016) 16114.
[43] K.L. Liu, C.H. Chao, H.C. Lee, C.S. Tsao, J. Fang, N.L. Wu, C.Y. Chao, A novel non-porous separator based on single-ion conducting triblock copolymer for stable lithium electrodeposition, J. Power Sources 419 (2019) 58–64.
[44] X.H. Rui, N. Ding, J. Liu, C. Li, C.H. Chen, Analysis of the chemical diffusion coefficient of lithium ions in $Li_3V_2(PO_4)_3$ cathode material, Electrochim. Acta 55 (2010) 2384–2390.
[45] H. Wu, Z. Yao, Q. Wu, S. Fan, C. Yin, C. Li, Confinement effect and air tolerance of Li plating by lithiophilic poly(vinyl alcohol) coating for dendrite-free Li metal batteries, J. Mater. Chem. 7 (2019) 22257–22264.
[46] N.W. Li, Y. Shi, Y.X. Yin, X.X. Zeng, J.Y. Li, C.J. Li, L.J. Wan, R. Wen, Y.G. Guo, A flexible solid electrolyte interphase layer for long-life lithium metal anodes, Angew. Chem. Int. Ed. 57 (2018) 1505–1509.
[47] G. Bieker, M. Winter, P. Bieker, Electrochemical in situ investigations of SEI and dendrite formation on the lithium metal anode, Phys. Chem. Chem. Phys. 17 (2015) 8670–8679.
[48] J.M. Ma, L. Fang, J. He, J.D. Liu, M.G. Wu, Y.Y. Hou, H.P. Wang, S.H. Qi, Q.H. Liu, J.W. Hu, Gradient solid electrolyte interphase and lithium ion solvation regulated by bisfluoroacetamide for stable lithium metal batteries, Angew. Chem. Int. Ed. (2021), https://doi.org/10.1002/anie.202013993.